ACS OMEGA

http://pubs.acs.org/journal/acsodf Article

# Chemometric Analysis of a Ternary Mixture of Caffeine, Quinic Acid, and Nicotinic Acid by Terahertz Spectroscopy

Phatham Loahavilai, Sopanant Datta, Kiattiwut Prasertsuk, Rungroj Jintamethasawat, Patharakorn Rattanawan, Jia Yi Chia, Cherdsak Kingkan, Chayut Thanapirom, and Taweetham Limpanuparb*

Cite This: *ACS Omega* 2022, 7, 35783−35791

Read Online

ACCESS | Metrics & More | Article Recommendations | Supporting Information

**ABSTRACT:** Caffeine, quinic acid, and nicotinic acid are among the significant chemical determinants of coffee quality. This study develops a chemometric model to quantify these compounds in ternary mixtures analyzed by terahertz time-domain spectroscopy (THz-TDS). A data set of 480 THz spectra was obtained from 80 samples. Combinations of data preprocessing methods, including normalization (*Z*-score, min-max scaling, Mie baseline removal) and dimensionality reduction (principal component analysis (PCA), factor analysis (FA), independent component analysis (ICA), locally linear embedding (LLE), non-negative matrix factorization (NMF), isomap), and prediction models (partial least-squares regression (PLSR), support vector regression (SVR), multilayer perceptron (MLP), convolutional neural network (CNN), gradient boosting) were analyzed for their prediction performance (totaling to 4,711,685 combinations). Results show that the highest quantification performance was achieved at a root-mean-square error of prediction (RMSEP) of 0.0254 (dimensionless mass ratio), using min-max scaling and factor analysis for data preprocessing and multilayer perceptron for prediction. Effects of preprocessing, comparison of prediction models, and linearity of data are discussed.

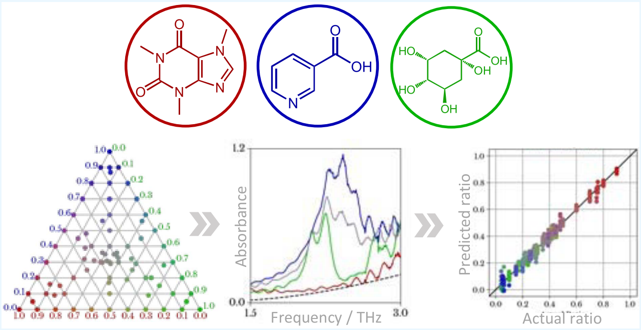

## 1. INTRODUCTION

Coffee is one of the most widely consumed and traded luxury goods in the world. Coffee plant belongs to the genus *Coffea* in the family *Rubiaceae*. The most economically important species are *Coffea arabica L.*, or arabica coffee, and *Coffea canephora var. robusta* (L. Linden), or robusta coffee. Coffee is mostly produced commercially from either species or blends of both.[1] Different blends of coffee with different degrees of roast vary by their body, mouthfeel, astringency, acidity, bitterness, flavors and aromas, and bioactive qualities.[2] These qualities are attributed to the chemical composition of each cup of coffee. Caffeine, quinic acid, and nicotinic acid (Figure 1) are among the major molecular determinants in coffee. The content of these compounds in coffee can vary significantly in the literature, depending on cultivar, processing, and method of analysis.

Caffeine, or 1,3,7-trimethyl-xanthine, plays physical, chemical, and biological roles in determining the strength and body of coffee, influencing the bitterness of coffee, and being psychologically active, respectively.[3] Caffeine can be found naturally in coffee beans, tea leaves, and cocoa beans and can be added to carbonated drinks, energy drinks, and other food and beverages.[4] The caffeine content in coffee beans ranges from 0.6 to 4% by dry mass.[3]

Quinic acid is one of the determining factors for the taste, flavor and aroma, and acidity of coffee.[5] As one of the major acids in coffee, it is found in green coffee beans and also derived from chlorogenic acids (CGAs) during the roasting process.[6] The content of quinic acid ranges from 0.33 to 0.85% by mass in green coffee beans.[7] Quinic acid content increases during the roasting process and is higher in darker roasted coffee due to a higher degree of CGA degradation. Quinic acid derivatives formed during the roasting process include bitter-tasting, flavor, and aroma compounds.[5]

Nicotinic acid (niacin; vitamin B3) is one of the micronutrients in coffee. It is a water-soluble B vitamin derived from trigonelline during coffee roasting. Coffee can be a significant dietary source of bioavailable nicotinic acid.[8] Nicotinic acid content ranges from 2 to 119 ppm by dry mass in coffee brews.[9] The amount of nicotinic acid produced varies with the degree of roasting.

**Received:** June 18, 2022
**Accepted:** September 15, 2022
**Published:** September 27, 2022

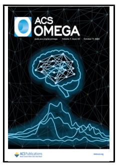

https://doi.org/10.1021/acsomega.2c03808

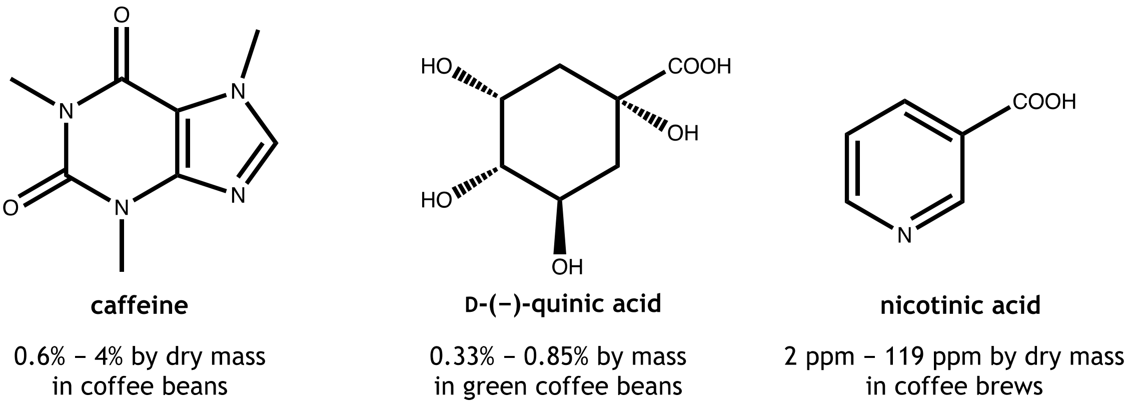

**Figure 1.** Chemical structure and content of caffeine, D-(−)-quinic acid, and nicotinic acid in coffee.

Terahertz time-domain spectroscopy (THz-TDS) coupled with chemometric analysis has recently gained attention as a rapid, nondestructive method of qualitative and quantitative determination of compounds in food products. The terahertz regime is in the frequency range of 0.1−10 THz, corresponding to the wavelength range of 0.03−3 mm. This range is located between the microwave and infrared ranges. THz spectroscopy can reveal crucial molecular information of intramolecular and intermolecular modes caused by hydrogen bonds, van der Waals energy, torsional modes, and vibrational modes of molecules.[10] THz waves have relatively low photon energy (4 meV for 1 THz; cf. 1.6−3.3 eV for visible light) and nonionizing penetration, causing minimal damage to biomolecules.[11] In addition, THz waves are resistant to strong scattering[12] and fluorescent substances[13] in samples, which are issues arising in infrared and Raman spectroscopy, respectively. THz-TDS has been used with chemometric methods, from simple linear regression[14,15] to machine learning models,[16−27] to quantify nutritional, pharmaceutical, and explosive compounds. Applications of THz-TDS and chemometric methods in food analysis are summarized in Table 1.

In this study, ternary mixtures of caffeine, quinic acid, and nicotinic acid are analyzed by THz-TDS and a chemometric model for the quantification of these compounds is developed. Combinations of preprocessing techniques and prediction models are assessed for their quantification performance.

## 2. RESULTS AND DISCUSSION

A series of 480 measurements of 80 samples with different compositions were analyzed by THz-TDS. Sample compositions were systematically and randomly determined, as shown in Figure 2. Replicate spectral measurements were conducted at different points on the samples. Further details can be found in Section 4.1.

Examples of the obtained absorbance spectra are shown in Figure 3. The THz spectra of pure compounds have been explored using experimental and computational methods and reported in the literature. The absorption peaks observed in Figure 3, especially those in the 2.0−3.0 THz range, are in good agreement with previous THz-TDS studies on caffeine,[28] quinic acid,[29] and nicotinic acid.[30]

The $k$-fold cross-validation method was used to evaluate the performance of each chemometric method. Spectra of ternary mixtures ($n$ = 300) were divided into five parts (each with $n$ = 60), whereby one part is in the test set and the rest are in the training set of each fold (e.g., part one is the test set of fold one, part two is the test set of fold two, etc.). Spectra of unitary and binary mixtures ($n$ = 180) were always in the training sets. This is to resemble the use of the model in practice, whereby unitary and binary mixtures set boundaries (or extrema) for the (potentially nonlinear) interpolation of ternary mixtures. Each model was assessed using root-mean-square error of calibration (RMSEC), RMSE for the training set, and root-mean-square error of prediction (RMSEP), RMSE for the test set.

Multiple chemometric models were examined in this study, as shown in Figure 4. Absorbance spectra of 540 features or data points were used as high-dimensional inputs for the models. Two data preprocessing measures were explored to understand their effect on the performance of the models. Normalization is

**Table 1. Recent Studies of THz-TDS Coupled with Chemometric Methods in Food Analysis**

| compound | sample matrix[a] | chemometric method[b] | reference |
|---|---|---|---|
| citric acid, D-(−)-fructose, D-(+)-lactose | n/a | PLSR, ANN | ref 16 |
| imidacloprid | rice powder | PLSR, SVR, iPLS, biPLS | ref 18 |
| L-(−)-glutamic acid, L-(−)-glutamine, L-(−)-tyrosine | cereal (foxtail millet) | PLSR, SVM | ref 20 |
| L-(−)-glutamic acid, L-(−)-glutamine, L-(−)-tyrosine | cereal (foxtail millet) | TM-stepwise regression, PLSR, N-PLSR | ref 21 |
| imidacloprid, carbendazim | flour | PLSR, PCA, SVM | ref 22 |
| D-(−)-fructose, D-(+)-galactose, D-(+)-mannose | n/a | PLSR, SVR | ref 23 |
| benzoic acid | flour | GRNN, BPNN | ref 24 |
| flavanoids | n/a | PLSR, ANN, PCA, SVM | ref 25 |
| proteins | soybean | PLSR, PCA-RBFNN, ABC-SVR | ref 26 |
| bisphenol A, bisphenol S, bisphenol AF, bisphenol E | n/a | SVR | ref 27 |
| caffeine, D-(−)-quinic acid, nicotinic acid | n/a | PLSR, SVR, MLP, CNN, gradient boost | this work |

[a] Reported as n/a if pure samples with binder (polyethylene) are used. [b] PLSR, partial least-squares regression; ANN, artificial neural networks; SVR, support vector regression; iPLS, interval partial least squares; biPLS, backward interval partial least squares; SVM, support vector machine; TM, Tchebichef image moment; N-PLSR, N-way partial least-squares regression; PCA, principal component analysis; GRNN, generalized regression neural network; BPNN, backpropagation neural network; RBFNN, radial basis function neural network; ABC, artificial bee colony; MLP, multilayer perceptron; and CNN, convolutional neural network.

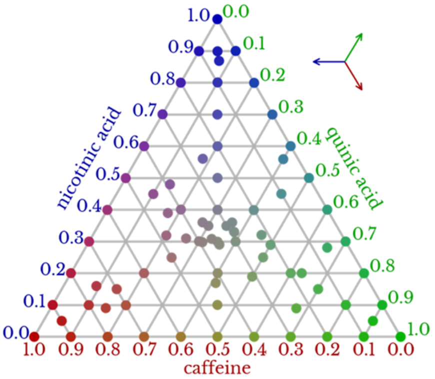

**Figure 2.** Ternary diagram of 80 sample compositions analyzed by THz-TDS. To read the mixture compositions (dimensionless mass ratio), the key on the top right can be placed on a point, extending the lines to the axes or triangle edges. Preparation methods are described in Section 4.1.

performed to ensure faster convergence, and dimensionality reduction techniques were performed to remove noises and only retain meaningful features. Each preprocessing step (normalization and dimensionality reduction) provides a bypass (no preprocessing) configuration, so each prediction model can have (1) both normalization and dimensionality reduction, (2) only normalization, (3) only dimensionality reduction, and (4) no preprocessing. Three normalization techniques, six dimensionality reduction techniques, and five prediction models were investigated in this study (see details in Section 4.2).

A list of chemometric models (combinations of preprocessing techniques and prediction models) with their respective RMSE values can be found in the Supporting Information. Preprocessing techniques resulting in the lowest RMSEP in each prediction model are shown in Table 2. Note that the best-performing PLSR (linear model) utilizes a nonlinear dimensionality reduction method. The nonlinear effect is further explained in Section 2.3. The lowest RMSEP of 0.0254 was achieved with the combination of min-max scaling, FA, and MLP prediction. The prediction performance of this model is visualized in Figure 5. The physical interpretation of parameters is not explicit in most of the investigated models due to the multiple layers of processing. A spectral feature may seem significant in a layer, yet be discarded in subsequent layers.

### 2.1. Effect of Preprocessing.

Data preprocessing measures are performed to improve the performance of prediction models. However, these techniques might not always improve the prediction performance. In some instances, they can remove useful features and correlations that are beneficial to the prediction model. As shown in Table 2, the CNN and gradient boosting models performed best without dimensionality reduction. The best CNN prediction was achieved when coupled with Mie baseline removal, with an RMSEP value of 0.0293. The CNN model without data preprocessing, on the other hand, resulted in a slightly higher RMSEP value of 0.0302. This shows how prediction models like CNN may already be able to extract useful features and data correlations without the need for data preprocessing, especially when the sample size is sufficient.

The effects of different data preprocessing methods on prediction performance are examined. The RMSEPs of models with one or more preprocessing techniques (normalization and/or dimensionality reduction) were compared to the corresponding combination with one of the techniques not applied. For example, to examine the effect of the min-max scaling normalization technique, the RMSEP of each model with no normalization is subtracted from the RMSEP of the model with the min-max scaling and the same dimensionality reduction and prediction models. A negative value of this difference signifies a reduction in RMSEP, hence an improvement in the prediction performance. Mean differences for each model are reported in Table 3. RMSE values of models with no preprocessing and plots of differences can be found in the Supporting Information.

PLSR with PCA preprocessing is among the most widely used chemometric model. In this study, implementing PCA preprocessing with PLSR led to a mean RMSEP reduction of 0.0026, compared to the PLSR model with no dimensionality reduction. This improvement can be attributed to how PCA maximizes the covariance among the input data, while PLSR maximizes the covariance between the input and output. PCA can be perceived as a filtering layer that discards noise, which can aid the covariance maximization of PLSR. Nevertheless, other nonlinear dimensionality reduction techniques like FA and ICA resulted in greater RMSEP reduction for PLSR models. Therefore, it can be beneficial to explore less common preprocessing techniques to improve the performance of prediction models. For normalization techniques, Mie baseline removal performs relatively well on average for all models.

Data preprocessing techniques resulted in reductions as well as increases in RMSEP. The increases can be attributed to how, in some instances, preprocessing can discard useful features that compromise the performance of prediction models. It is

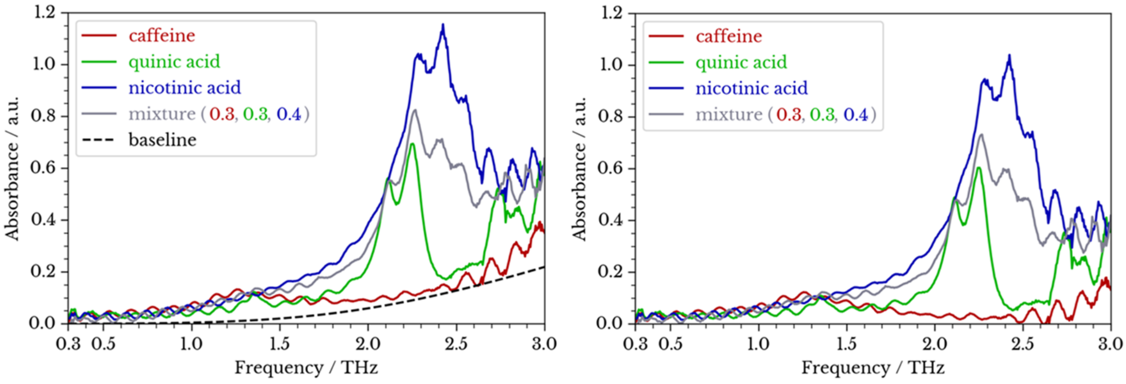

**Figure 3.** THz absorption spectra of pure caffeine, quinic acid, nicotinic acid, and a ternary mixture before (left) and after (right) Mie baseline removal (a.u. = arbitrary unit).

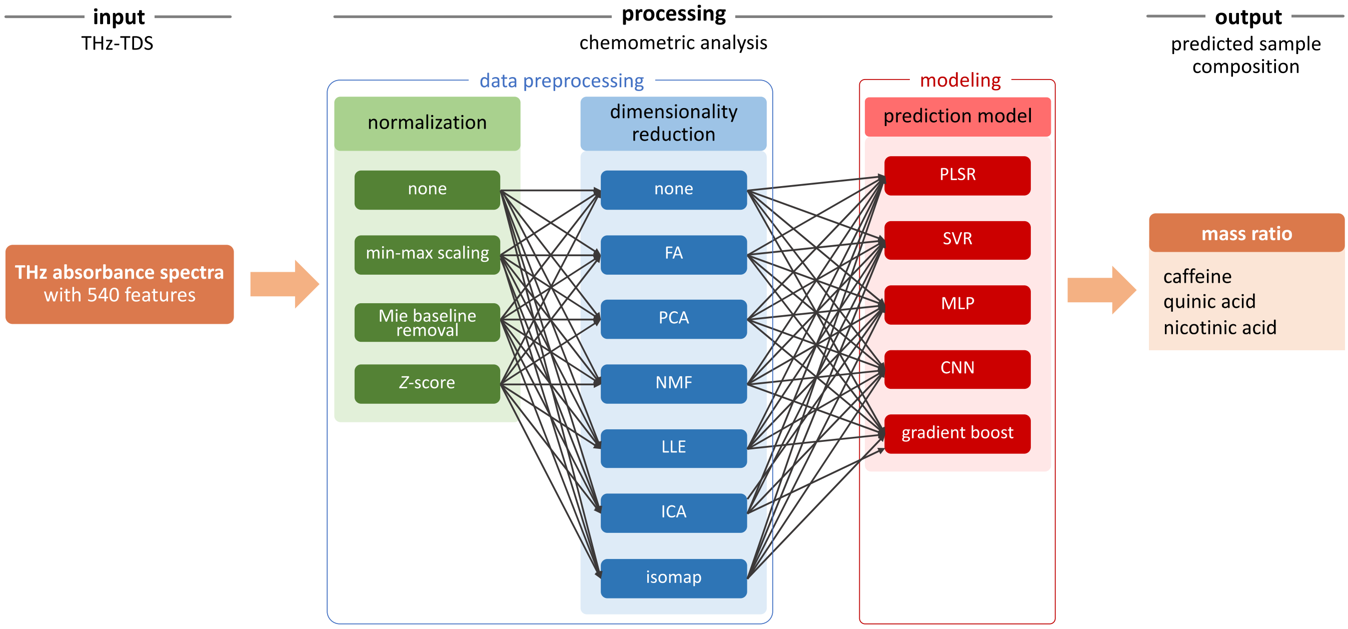

**Figure 4.** Pipeline of chemometric methods. See the list of abbreviations in Table 4.

**Table 2. Highest-Performance Preprocessing Technique by RMSEP for Each Prediction Model and Their Respective Optimal Hyperparameters**[a]

| model | normalization | dimensionality reduction | RMSEC | RMSEP |
|---|---|---|---|---|
| MLP | min-max scaling | FA | 0.0213 | 0.0254 |
| #neurons: 4, activation fn: logistic, solver: lbfgs | | 27 components | | |
| SVR | Mie baseline removal | PCA | 0.0262 | 0.0260 |
| type: NuSVR, nu: 0.5, C: 1.0, iterations: 2000, kernel: rbf, $\gamma$: auto | multifactor | 27 components | | |
| CNN | Mie baseline removal | none | 0.0276 | 0.0293 |
| activation fn: sigmoid | multifactor (with factor concatenation) | | | |
| gradient boosting | Mie baseline removal | none | 0.0214 | 0.0316 |
| learning rate: 0.01, max depth: 5, min child weight: 2, $\gamma$: 0, subsample: 0.3, colsample_bytree: 0.6, num_round: 10,000 | multifactor | | | |
| PLSR | Mie baseline removal | LLE | 0.0312 | 0.0283 |
| with prescale, 3 components | multifactor | modified with 14 components, 30 neighbors | | |

[a] Abbreviations are listed in Table 4. RMSEC and RMSEP values are reported as dimensionless mass ratios.

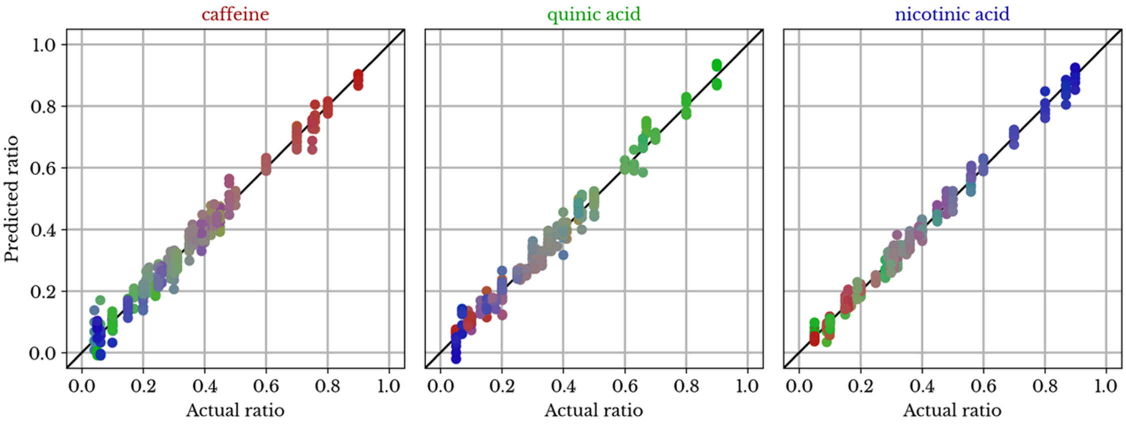

**Figure 5.** Performance of MLP with min-max scaling and FA preprocessing: predicted vs actual (dimensionless) mass ratio of caffeine (red), quinic acid (green), and nicotinic acid (blue) in ternary mixtures (point colors are proportional to their associated predicted composition—see Figure 2).

important to select the right combinations of preprocessing techniques and prediction models to enhance the effectiveness of each process and optimize the prediction performance.

### 2.2. Prediction Model.

The combinations of data preprocessing methods resulting in the best prediction performance for each model are shown in Table 2. PLSR is a widely used

Table 3. Mean Change in RMSEP for Each Prediction Model by Different Preprocessing Methods[a]

| preprocessing technique | | mean change in RMSEP | | | | |
|---|---|---|---|---|---|---|
| | | PLSR | SVR | MLP | CNN | gradient boost |
| normalization | Mie baseline removal | −0.3326 | −0.1252 | −0.0063 | −0.0087 | −0.0071 |
| | min-max scaling | −0.0866 | 0.3918 | 0.0088 | 0.0144 | 0.0130 |
| | *Z*-score | 0.0732 | 1.0256 | 0.0282 | 0.0273 | 0.0240 |
| dimensionality reduction | FA | −0.0047 | −0.3354 | −0.0109 | 0.0249 | 0.0055 |
| | ICA | −0.0037 | −0.3356 | 0.0312 | 0.0443 | 0.0114 |
| | isomap | 0.0229 | 0.6478 | 0.0108 | 0.0316 | 0.0239 |
| | LLE | −0.0021 | −0.4042 | 0.0305 | 0.0080 | 0.0097 |
| | NMF | 0.0001 | −0.4179 | 0.0118 | 0.0129 | 0.0080 |
| | PCA | −0.0026 | 0.9325 | −0.0050 | 0.0133 | 0.0119 |

[a] RMSEP values are reported as dimensionless mass ratios.

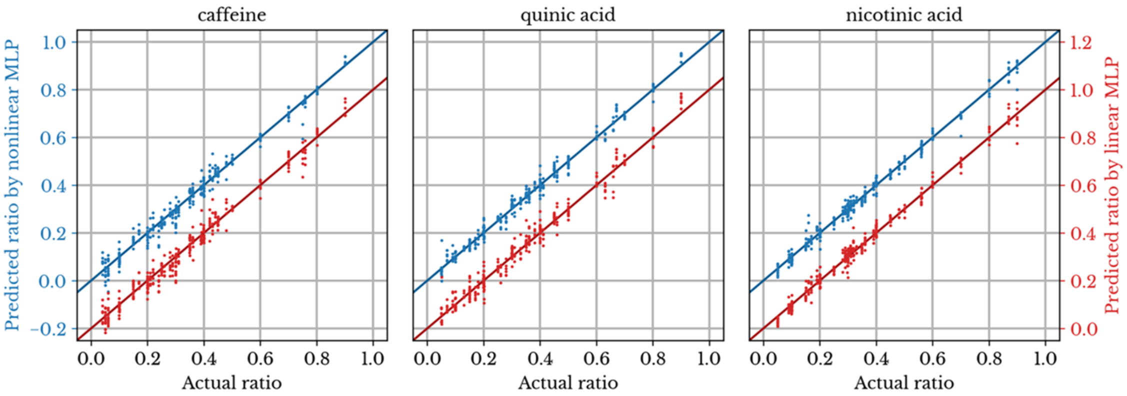

**Figure 6.** Prediction performance of nonlinear (blue) and linear (red) MLP models for (dimensionless) mass ratios of caffeine, quinic acid, and nicotinic acid in ternary mixtures. The left vertical axis is shifted up with respect to the right vertical axis for ease of comparison.

machine learning model, and PCA is among the most common dimensionality reduction methods used with it. According to the results, Mie baseline removal and LLE preprocessing resulted in the best-performing PLSR prediction with an RMSEP of 0.0282, while Mie baseline removal and PCA preprocessing resulted in a higher RMSEP of 0.0292. Thus, according to this study, PLSR prediction can be optimized by data preprocessing of Mie baseline removal and LLE modified with 14 components and 30 neighbors.

**2.3. Linearity of Data.** The linearity between the input (spectral data) and output (mixture composition) was investigated. This was done by modifying the activation function in the hidden layer and output layer ("tanh" function for nonlinear model and "identity" function for linear model) of the MLP model. Linear and nonlinear MLP models with no preprocessing are compared. The best nonlinear MLP model has a 14% lower RMSEP compared to the linear model (0.0270 vs 0.0316). The prediction performances of these models are visualized in Figure 6. The MLP nonlinear models resulted in lower RMSEP values than those of the linear models in most cases. (see the Supporting Information). This suggests a nonlinear relationship between our input data and mixture composition.

## 3. CONCLUSIONS

In this study, ternary mixtures of caffeine, quinic acid, and nicotinic acid with varying compositions were analyzed by THz-TDS, and chemometric models were investigated for their performance in the prediction of mixture compositions. The performance of different prediction models, as well as the effect of different data preprocessing techniques on the performance, was explored. Among all models, MLP with the preprocessing techniques of min-max scaling and factor analysis (with 27 components) had the best prediction performance with a dimensionless mass ratio RMSEP of 0.0254. The widely used PLSR prediction model achieved its best prediction results when Mie baseline removal and LLE dimensionality reduction were performed. In addition, a nonlinear model resulted in better prediction performance than the linear model, using MLP as a model method.

The developed chemometric models can serve as a stepping stone for further investigation in food, pharmaceutical, and cosmetic products containing these compounds, such as coffee, energy drinks, and supplements. Additional practical considerations should be taken into account when applying the techniques to the products.

## 4. MATERIALS AND METHODS

**4.1. THz-TDS Spectroscopy.** All chemicals used are analytical grade (>98% purity) and in their anhydrous forms. Caffeine was purchased from LobaChemie; D-(−)-quinic acid and nicotinic acid were obtained from Sigma-Aldrich. A high-density polyethylene (HDPE) powder purchased from Sigma-Aldrich was used as the binder for all sample mixtures. All chemicals were used as received without any further purification.

The mixture compositions shown in Figure 2 include 60 and 20 systematically and randomly determined compositions, respectively. The systematically determined compositions include 10 points evenly spaced on each of the three edges and three medians of the ternary diagram (triangle). Each sample was mixed with HDPE at a 20:80 mass ratio and ground to avoid aggregates and heterogeneous clusters. Each mixture

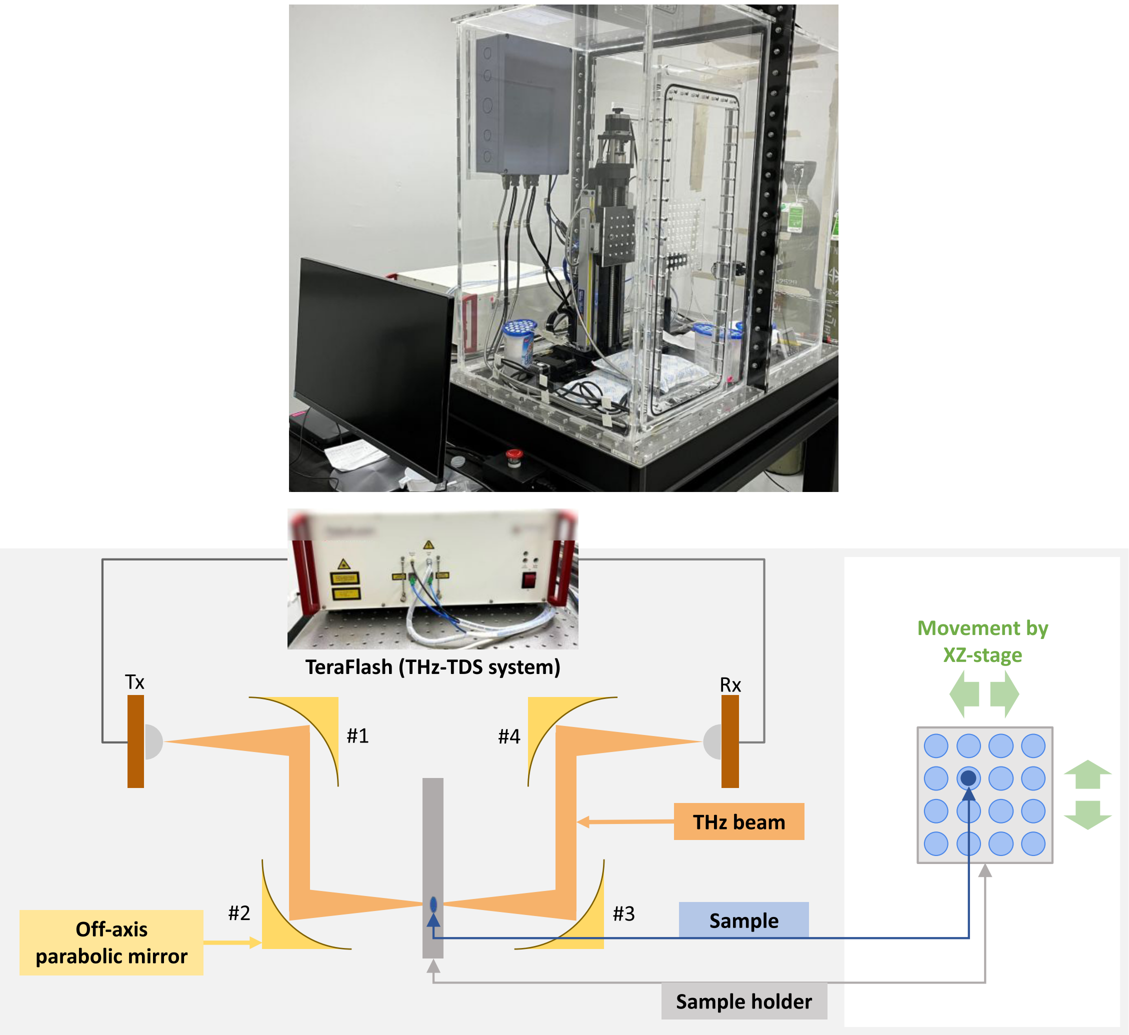

**Figure 7.** Custom-made THz-TDS system at NECTEC, Pathum Thani, Thailand. The photoconductive antenna transmitter and receiver are labeled as Tx and Rx, respectively. Off-axis parabolic mirrors are labeled as #1, #2, #3, and #4.

was transferred to a hydraulic press to be formed into disc pellets at 7 tons for 5 min. Each disc pellet had an approximately 100 mg of weight, 13 mm of diameter, and 0.850−0.950 mm of thickness. In addition to the samples, pure HDPE was prepared to be used as a blank (reference).

Six spectral measurements of each composition were performed for a total of 480 spectra. Each measurement was performed at different points on the samples. Four measurement points were arranged in a square shape, and two measurement points (the first and the last) were placed in the center of the square, 1.0 mm apart from the other four.

Absorption spectra of the range 0.3−3.0 THz were obtained from a THz-TDS system (TeraFlash, TOPTICA Photonics AG, Germany), as shown in Figure 7. The source of radiation is a photoconductive switch generated by a femtosecond laser at 780 nm. The experiment was conducted at an air-conditioned room temperature (25 ± 2 °C). The acrylic chamber with a nitrogen-purged atmosphere (relative humidity ≤5%) was custom-made by researchers at the National Electronics and Computer Technology Center (NECTEC), Thailand. The spectra were acquired at a 5 GHz resolution, optimized, and formed a time-domain data set $\{x_i, y_i \mid x_i \in \mathbf{R}^{4001}, y_i \in \mathbf{R}^3, i = 1, 2, \cdots, n\}$ of $n$ samples, where each sample contained vector $x_i$ and target concentration $y_i$. Each time-domain spectrum was obtained from a 2000-sample moving average. For background compensation, frequency-domain data were subtracted from the reference spectra.

### 4.2. Chemometric Models.

Data preprocessing methods of normalization (three techniques) and dimensionality reduction (six techniques) and five prediction models were explored in this study, as described in Table 4. An exhaustive investigation of hyperparameters for each preprocessing technique and prediction model was conducted to identify the optimal hyperparameters reported in Table 2. A total of 4,711,685 combinations of preprocessing techniques and models were explored. Additionally, a novel Mie baseline removal method in the form of convex optimization is proposed and used in this study, as described in Table 4.

Source codes were implemented using Python and the scikit-learn,[31] Keras,[32] and XGBoost[33] Python libraries. Jupyter notebook was used as the integrated development environment. Optimization of hyperparameters was performed on ray.io. All data and source codes are available in the Supporting Information. The total runtime for our computational investigation described in the paper is approximately 3 days on AWS Graviton 2 (256 cores, 1 TB RAM). However, an individual model can be computed locally on a standard workstation (4 cores, 8 GB RAM) in less than 1 hour.

Table 4. List of Investigated Chemometric Techniques with Brief Description

| process | technique | description |
|---|---|---|
| normalization | *Z*-score | features are transformed so that the mean is 0 and the standard deviation is 1. |
| | min-max scaling | features are transformed so that data is in the range of [0, 1]. |
| | Mie baseline removal | Mie scattering caused by the interaction of the HDPE binder with THz waves is corrected.<br>Mie efficiency ($Q_{ext}$) for multiple wavelengths was generated by Matzler.[34] In this study, the baseline is calculated as $\xi \cdot Q_{ext}$, where $\xi$ is a coefficient computed such that the baseline is at the troughs.<br>we regarded this as a convex optimization problem to a valid set of discretized angular frequencies $\Omega$, which excludes the water peaks (with ±25 GHz bandwidth) and the frequencies ranging from 0.3 to 0.55 THz due to negative absorbance residues arising from noises. We denoted absorbance as $a(\omega)$ and baseline as $\xi \cdot Q_{ext}(\omega)$. The optimization target was to minimize the following.<br>$\sum_{\omega \in \Omega} \begin{cases} (a(\omega) - \xi \cdot Q_{ext}(\omega))^2; & a(\omega) > \xi \cdot Q_{ext}(\omega) \\ M(\xi \cdot Q_{ext}(\omega) - a(\omega))^2, & \text{otherwise} \end{cases}$<br>$\xi$ is the solution found after optimization. $M$ is an arbitrarily large number to keep the baseline from exceeding the spectra troughs.<br>○ for single-factor, $\xi$ is a constant scalar value. Minimum $\xi$ computed in a training set is used among all spectra, including the test set.<br>○ for multifactor, $\xi$ can have different values, and the baseline of each spectrum is individually removed. A special case of multifactor concatenates the $\xi$ parameters after dimensionality reductor as another feature. |
| dimensionality reduction | principal component analysis (PCA) | data is projected onto a low-dimensional linear space formed by principal orthogonal components.<br>cumulative variance in the predictors is explained. |
| | factor analysis (FA) | data is projected onto a low-dimensional linear space formed by factors that correlate with other variables.<br>correlations between variables are explained. |
| | independent component analysis (ICA) | data is projected onto a low-dimensional linear space formed by maximally independent components. |
| | locally linear embedding (LLE) | data is projected onto a low-dimensional nonlinear space, preserving distances between neighboring points. |
| | non-negative matrix factorization (NMF) | data is projected onto a low-dimensional linear space formed by non-negative additive factors. |
| | isomap | data is projected onto a low-dimensional nonlinear space, preserving geodesic distances. |
| prediction model | partial least-squares regression (PLSR) | least-squares regression is performed on dimensionally reduced input data with the retained correlation between data. |
| | support vector regression (SVR) | hyperplane parameters, whose margin of error confines as many training data points as possible, are obtained and used for prediction. Outliers tend to be far away from the margin of error. |
| | multilayer perceptron (MLP) | nonlinear function approximator is obtained for either classification or regression, and parameters are adjusted using "back-propagation". Hidden and output layers contain neurons using an activation function. Data is fed from one layer to another. |
| | convolutional neural network (CNN) | nonlinear mapping function (residual block[24]) between the input and output is obtained. Data features are extracted through the convolution of input and filters. |
| | gradient boosting | model is developed from a combination of trained base learners. XGBoost is an optimized distributed gradient boosting library that has regularization parameters to prevent overfitting and was selected in this study. |

## ■ ASSOCIATED CONTENT

### Data Availability Statement

The prediction performance of all of the investigated models can be accessed via Open Science Framework (OSF), at DOI: 10.17605/OSF.IO/3YXBU.

### Supporting Information

The Supporting Information is available free of charge at https://pubs.acs.org/doi/10.1021/acsomega.2c03808.

Distribution of change in the RMSE of each prediction model using different normalization techniques and dimensionality reduction techniques for preprocessing, and highest-performance RMSEP for each prediction model with no preprocessing and their respective optimal hyperparameters (ZIP)

Raw time-domain and processed frequency-domain spectral data and source codes in Jupyter notebooks for data extraction and analysis, including a test case from the best performing models (ZIP)

## ■ AUTHOR INFORMATION

### Corresponding Author

**Taweetham Limpanuparb** − *Mahidol University International College, Mahidol University, Nakhon Pathom 73170, Thailand;* orcid.org/0000-0002-8558-6199; Email: taweetham.lim@mahidol.edu

### Authors

**Phatham Loahavilai** − *National Electronics and Computer Technology Center, Pathum Thani 12120, Thailand; Department of Engineering Physics, Tsinghua University, Beijing 100084, China;* orcid.org/0000-0001-8118-1576

**Sopanant Datta** − *Mahidol University International College, Mahidol University, Nakhon Pathom 73170, Thailand;* orcid.org/0000-0001-8042-4513

**Kiattiwut Prasertsuk** − *National Electronics and Computer Technology Center, Pathum Thani 12120, Thailand;* orcid.org/0000-0003-3798-9935

**Rungroj Jintamethasawat** − *National Electronics and Computer Technology Center, Pathum Thani 12120, Thailand*

**Patharakorn Rattanawan** − *National Electronics and Computer Technology Center, Pathum Thani 12120, Thailand*

**Jia Yi Chia** − *National Electronics and Computer Technology Center, Pathum Thani 12120, Thailand;* orcid.org/0000-0001-5538-5030

**Cherdsak Kingkan** − *National Electronics and Computer Technology Center, Pathum Thani 12120, Thailand*

**Chayut Thanapirom** − *National Electronics and Computer Technology Center, Pathum Thani 12120, Thailand*

Complete contact information is available at: https://pubs.acs.org/10.1021/acsomega.2c03808

### Notes

The authors declare no competing financial interest.

## ■ ACKNOWLEDGMENTS

T.L. was supported by a mid-career researcher development grant (NRCT5-RSA63015-22) jointly funded by the National Research Council of Thailand (NRCT) and Mahidol University. He also received MU-GPI grant (Contract No. 06/2565) from the university. J.Y.C. was supported by the National Electronics and Computer Technology Center (NECTEC; P2150039). K.P. was supported by the National Science and Technology Development Agency (NSTDA)'s Food and Feed Innovation Center (P1850906). Funders had no role in study design, data collection and analysis, decision to publish, or preparation of the manuscript. The authors thank Napat Cota, Natcha Cota, and Piyaphat Phukphan for constructing the THz-TDS chamber and the operating software and Junming Ho for discussions on the possibility of THz-TDS spectral simulation by computational methods. Siriyakorn Chudhakorn's cover art is gratefully appreciated. The authors are thankful for comments and suggestions by seven reviewers and the editorial office staff.

## ■ REFERENCES

(1) Alcantara, G. M.; Dresch, D.; Melchert, W. R. Use of non-volatile compounds for the classification of specialty and traditional Brazilian coffees using principal component analysis. *Food Chem.* **2021**, *360*, No. 130088.

(2) Cheng, B.; Furtado, A.; Smyth, H. E.; Henry, R. J. Influence of genotype and environment on coffee quality. *Trends Food Sci. Technol.* **2016**, *57*, 20−30.

(3) Oestreich-Janzen, S. Chemistry of Coffee. In *Comprehensive Natural Products II*; Liu, H.-W.; Mander, L. Eds.; Elsevier: Oxford, England, 2010; Vol. 3, pp 1085−1117.

(4) Reyes, C. M.; Cornelis, M. C. Caffeine in the Diet: Country-Level Consumption and Guidelines. *Nutrients* **2018**, *10*, No. 1772.

(5) Gigl, M.; Frank, O.; Barz, J.; Gabler, A.; Hegmanns, C.; Hofmann, T. Identification and Quantitation of Reaction Products from Quinic Acid, Quinic Acid Lactone, and Chlorogenic Acid with Strecker Aldehydes in Roasted Coffee. *J. Agric. Food Chem.* **2021**, *69*, 1027−1038.

(6) Shibamoto, T. Volatile Chemicals from Thermal Degradation of Less Volatile Coffee Components. In *Coffee in Health and Disease Prevention*; Preedy, V. R. Ed.; Academic Press: San Diego, USA, 2015; Chapter 2, pp 129−135.

(7) Moon, J.-K.; Shibamoto, T. Formation of Volatile Chemicals from Thermal Degradation of Less Volatile Coffee Components: Quinic Acid, Caffeic Acid, and Chlorogenic Acid. *J. Agric. Food Chem.* **2010**, *58*, 5465−5470.

(8) Perrone, D.; Donangelo, C. M.; Farah, A. Fast simultaneous analysis of caffeine, trigonelline, nicotinic acid and sucrose in coffee by liquid chromatography−mass spectrometry. *Food Chem.* **2008**, *110*, 1030−1035.

(9) Jeszka-Skowron, M.; Frankowski, R.; Zgoła-Grześkowiak, A. Comparison of methylxantines, trigonelline, nicotinic acid and nicotinamide contents in brews of green and processed Arabica and Robusta coffee beans − Influence of steaming, decaffeination and roasting processes on coffee beans. *LWT* **2020**, *125*, No. 109344.

(10) Baxter, J. B.; Guglietta, G. W. Terahertz Spectroscopy. *Anal. Chem.* **2011**, *83*, 4342−4368.

(11) Qin, J.; Ying, Y.; Xie, L. The Detection of Agricultural Products and Food Using Terahertz Spectroscopy: A Review. *Appl. Spectrosc. Rev.* **2013**, *48*, 439−457.

(12) Lu, S.; Zhang, X.; Zhang, Z.; Yang, Y.; Xiang, Y. Quantitative measurements of binary amino acids mixtures in yellow foxtail millet by terahertz time domain spectroscopy. *Food Chem.* **2016**, *211*, 494−501.

(13) Li, Y.-S.; Church, J. S. Raman spectroscopy in the analysis of food and pharmaceutical nanomaterials. *J. Food Drug Anal.* **2014**, *22*, 29−48.

(14) Datta, S.; Prasertsuk, K.; Khammata, N.; Rattanawan, P.; Chia, J. Y.; Jintamethasawat, R.; Chulapakorn, T.; Limpanuparb, T. Terahertz Spectroscopic Analysis of Lactose in Infant Formula: Implications for Detection and Quantification. *Molecules* **2022**, *27*, No. 5040.

(15) Cheng, H.; Huang, H.-c.; Yang, M.-f.; Yang, M.-h.; Yan, H.; Panezai, S.; Zheng, Z.-Y.; Zhang, Z.; Zhang, Z.-l. Characterization of the remediation of chromium ion contamination with bentonite by terahertz time-domain spectroscopy. *Sci. Rep.* **2022**, *12*, No. 11149.

(16) El Haddad, J.; de Miollis, F.; Bou Sleiman, J.; Canioni, L.; Mounaix, P.; Bousquet, B. Chemometrics Applied to Quantitative

Analysis of Ternary Mixtures by Terahertz Spectroscopy. *Anal. Chem.* **2014**, *86*, 4927−4933.

(17) Sleiman, J. B.; Haddad, J. E.; Perraud, J. B.; Bassel, L.; Bousquet, B.; Palka, N.; Mounaix, P. In*Qualitative and Quantitative Analysis of Explosives by Terahertz Time-Domain Spectroscopy: Application to Imaging*, 39th International Conference on Infrared, Millimeter, and Terahertz waves (IRMMW-THz), 2014; pp 1−2.

(18) Chen, Z.; Zhang, Z.; Zhu, R.; Xiang, Y.; Yang, Y.; Harrington, P. B. Application of terahertz time-domain spectroscopy combined with chemometrics to quantitative analysis of imidacloprid in rice samples. *J. Quant. Spectrosc. Radiat. Transfer* **2015**, *167*, 1−9.

(19) Yehia, A. M.; Mohamed, H. M. Chemometrics resolution and quantification power evaluation: Application on pharmaceutical quaternary mixture of Paracetamol, Guaifenesin, Phenylephrine and *p*-aminophenol. *Spectrochim. Acta, Part A* **2016**, *152*, 491−500.

(20) Zhang, X.; Lu, S.; Liao, Y.; Zhang, Z. Simultaneous determination of amino acid mixtures in cereal by using terahertz time domain spectroscopy and chemometrics. *Chemom. Intell. Lab. Syst.* **2017**, *164*, 8−15.

(21) Lu, S. H.; Li, B. Q.; Zhai, H. L.; Zhang, X.; Zhang, Z. Y. An effective approach to quantitative analysis of ternary amino acids in foxtail millet substrate based on terahertz spectroscopy. *Food Chem.* **2018**, *246*, 220−227.

(22) Cao, B.; Li, H.; Fan, M.; Wang, W.; Wang, M. Determination of pesticides in a flour substrate by chemometric methods using terahertz spectroscopy. *Anal. Methods* **2018**, *10*, 5097−5104.

(23) Du, C.; Zhang, X.; Zhang, Z. Quantitative analysis of ternary isomer mixtures of saccharide by terahertz time domain spectroscopy combined with chemometrics. *Vib. Spectrosc.* **2019**, *100*, 64−70.

(24) Sun, X.; Liu, J.; Zhu, K.; Hu, J.; Jiang, X.; Liu, Y. Generalized regression neural network association with terahertz spectroscopy for quantitative analysis of benzoic acid additive in wheat flour. *R. Soc. Open Sci.* **2019**, *6*, No. 190485.

(25) Yin, M.; Wang, J.; Huang, H.; Huang, Q.; Fu, Z.; Lu, Y. Analysis of Flavonoid Compounds by Terahertz Spectroscopy Combined with Chemometrics. *ACS Omega* **2020**, *5*, 18134−18141.

(26) Wei, X.; Li, S.; Zhu, S.; Zheng, W.; Zhou, S.; Wu, W.; Xie, Z. Quantitative analysis of soybean protein content by terahertz spectroscopy and chemometrics. *Chemom. Intell. Lab. Syst.* **2021**, *208*, No. 104199.

(27) Sun, Y.; Huang, J.; Shan, L.; Fan, S.; Zhu, Z.; Liu, X. Quantitative analysis of bisphenol analogue mixtures by terahertz spectroscopy using machine learning method. *Food Chem.* **2021**, *352*, No. 129313.

(28) Otsuka, Y.; Ito, A.; Takeuchi, M.; Sasaki, T.; Tanaka, H. Effects of temperature on terahertz spectra of caffeine/oxalic acid 2:1 cocrystal and its solid-state density functional theory. *J. Drug Delivery Sci. Technol.* **2020**, *56*, No. 101215.

(29) Thanapirom, C.; Yi, C. J.; Cota, N.; Jintamethasawat, R.; Kusolthossakul, W.; Prasertsuk, K. In*An ADAM Optimization for Water-Vapor Effect Removal in THz-TDS Data*, 45th International Conference on Infrared, Millimeter, and Terahertz Waves (IRMMW-THz), 2020; pp 1−2.

(30) Ding, L.; Fan, W.-H.; Chen, X.; Chen, Z.-Y.; Song, C. Terahertz spectroscopy and solid-state density functional theory calculations of structural isomers: Nicotinic acid, isonicotinic acid and 2-picolinic acid. *Mod. Phys. Lett. B* **2017**, *31*, No. 1750149.

(31) Pedregosa, F.; Varoquaux, G.; Gramfort, A.; Michel, V.; Thirion, B.; Grisel, O.; Blondel, M.; Prettenhofer, P.; Weiss, R.; Dubourg, V. Scikit-learn: Machine learning in Python. *J. Mach. Learn. Res.* **2011**, *12*, 2825−2830.

(32) He, K.; Zhang, X.; Ren, S.; Sun, J. In *Deep Residual Learning for Image Recognition*, 2016 IEEE Conference on Computer Vision and Pattern Recognition (CVPR), 2016; pp 770−778.

(33) Chen, T.; Guestrin, C. In *XGBoost: A Scalable Tree Boosting System*, Proceedings of the 22nd ACM SIGKDD International Conference on Knowledge Discovery and Data Mining; Association for Computing Machinery: San Francisco, USA, 2016.

(34) Mätzler, C. *MATLAB Functions for Mie Scattering and Absorption*, version 2, 2002.

https://doi.org/10.1021/acsomega.2c03808